Time-Resolved Fluorescence of Glucagon Studied by Global Compartmental Analysis

Luc Van Dommelen,[†] Noël Boens,*[,†] and Marcel Ameloot[‡]

Department of Chemistry, Katholieke Universiteit Leuven, 3001 Heverlee-Leuven, Belgium, and Limburgs Universitair Centrum, 3590 Diepenbeek, Belgium

Received: November 12, 1997

The photophysics of the polypeptide hormone glucagon in aqueous phosphate buffer ($\lambda^{ex} = 295$ nm, pH 6.7, 17.2 °C) in the presence of the added quencher sodium iodide is investigated using standard simultaneous biexponential and global compartmental analyses of its fluorescence decay surface. The use of the scanning procedure in global compartmental analysis allows distinction between reversible and irreversible transformation processes in the excited state (*J. Phys. Chem.* **1995**, *99*, 8959−8971). Furthermore, by comparison of the species-associated with the decay-associated emission spectra, a unidirectional process in the excited state can be distinguished from the case where no interconversion occurs between the two excited-state species. Scanning different rate constants and comparing the species-associated with the decay-associated emission spectra indicate that the dual exponential fluorescence decays of the single tryptophan-containing polypeptide glucagon are due to two non-interconverting excited-state species resulting from excitation of their respective ground states. On the time scale of fluorescence there is no interconversion between the two excited-state species. The composite deactivation rate constant values for monomeric glucagon in phosphate buffer ($k_{01} = 1.01 \times 10^9$ s^{-1} and $k_{02} = 2.7 \times 10^8$ s^{-1}) are separated into contributions via fluorescence ($k_{F1} = 0.05 \times 10^9$ s^{-1} and $k_{F2} = 1.6 \times 10^8$ s^{-1}) and nonradiative processes ($k_{NR1} = 0.96 \times 10^9$ s^{-1} and $k_{NR2} = 1.1 \times 10^8$ s^{-1}). The fluorescence quantum yields in the absence of added quencher are $\phi^0_{F1} = 0.05$ and $\phi^0_{F2} = 0.58$. The relatively high values ($>1 \times 10^9$ M^{-1} s^{-1}) of the rate constants of quenching are indicative of a tryptophyl residue exposed to the surrounding aqueous environment. The obtained values of the rate constants may indicate that the decay component of 1 ns is associated with a tryptophyl residue in a flexible extended random coil conformation of the polypeptide chain while its 3.7 ns counterpart corresponds to a tryptophan in a compact, quite rigid backbone conformation. The method used to elucidate the origin of the biexponential fluorescence decays of glucagon is generally applicable to any intramolecular two-state excited-state process and will be useful in the study of peptides and proteins with dual exponential fluorescence decay kinetics.

Introduction

Time-resolved tryptophyl fluorescence spectroscopy provides detailed dynamic structural information about proteins.[1] Significantly improved procedures for simultaneous data analysis of fluorescence decay surfaces[2,3] are useful tools for investigating the excited-state kinetics of tryptophan, tryptophyl polypeptides, and proteins. Indeed, the recently developed global compartmental analysis approach with quenching[3] allows one, in the absence of any foreknowledge, to specify upper and lower bounds on the four rate constants describing the kinetics of intramolecular two-state excited-state processes by means of the scanning procedure. At least three different quencher concentrations are needed, and the two quenching rate constants must be different.[3] Additionally, the steady-state fluorescence spectrum can be resolved into unique species-associated spectra. This new analysis method also makes it possible to distinguish reversible from irreversible intramolecular two-state excited-state processes.[3] Moreover, without *a priori* information, one can distinguish between competing models for irreversible intramolecular two-state excited-state processes, i.e., a unidirectional excited-state process or no excited-state process.[3] We have used the new global compartmental analysis approach with quenching in the absence of foreknowledge[3] to show that the biexponential fluorescence decays of tryptophan zwitterion[4−14] in aqueous solution originate from a reversible two-state excited-state process whereby the corresponding ground-state species are excited.[15]

Glucagon is a hormone, consisting of a linear polypeptide of 29 amino acid residues with a single tryptophan (Trp) at position 25, that regulates glycogenolysis and glyconeogenesis in the liver. Extensive attention has been focused on the conformation of glucagon in single crystals and in solution. Since only studies of monomeric glucagon in aqueous solution are relevant to our investigation, studies of trimeric and/or crystalline glucagon will not be discussed. Circular dichroism (CD) spectra have been interpreted to indicate that monomeric glucagon in dilute aqueous solution exists predominantly as a flexible "random coil" but with about 15−20% α-helical structure.[16] Using ^{1}H NMR (100 and 270 MHz), Wagman *et al.* found that the chemical shifts characteristic for monomeric glucagon are not fully identical with those expected for a random coil structure, indicating some characteristic structure with low internal mobility near the carboxy-terminal region (residues 22−29).[17] High-resolution ^{1}H NMR (360 MHz) studies[18] confirmed that

* To whom correspondence should be addressed. Tel.: ++/32/16/327497. Fax: ++/32/16/327990. E-mail: Noel.Boens@chem.kuleuven.ac.be.
† Katholieke Universiteit Leuven.
‡ Limburgs Universitair Centrum.

S1089-5647(98)00170-9 CCC: $15.00
Published on Web 04/04/1998

monomeric glucagon in dilute aqueous solution adopts predominantly an extended flexible conformation which, however, contains a local nonrandom chain-fold involving fragment 22−25. On the basis of a comparison with the pentapeptide fragment 22−26, Boesch *et al.* concluded that this local, quite rigid backbone conformation adjacent to Trp_{25} is different from an α-helix. This nonrandom spatial structure occurs in approximately 20% of the molecular population at ambient temperature.[18] Ross *et al.* have shown by optically detected magnetic resonance and phosphorescence that the structural environment of Trp_{25} is different in the 22−26 fragment than in intact glucagon, so that the extrapolation from fragment to whole molecule cannot be made.[19] Their results are consistent with the published CD results[16] for α-helical structure in the 18−29 region of the hormone. Evidence that glucagon in dilute acid solution (pH 3) is stabilized by intrachain interactions is given by McBride-Warren and Epand,[20] who showed that some 25−30% of the exchangeable amide hydrogens exchange about 10 times more slowly than in randomly coiled polypeptides, suggesting a compact, well-defined nonrandom structure. This is consistent with the presence of a stable helix of approximately two turns.[16,19] Hydrogen−deuterium exchange experiments monitored by ^{1}H NMR (500 MHz) showed that the backbone amide NHs form intrastrand hydrogen bonds, suggesting the existence of some degree of compact structure of monomeric glucagon in acid solution.[21] The small J coupling constants arising from interactions between 6 amide NHs and C_αHs imply a helical structure.[21] The model for the three-dimensional structure of glucagon in dilute aqueous solution proposed by Korn and Ottensmeyer[22] shows a well-defined structure for glucagon with β-turns located at residues 2−5, 10−13, and 15−18, β-sheet from 5 to 10, and α-helix from 19 to 27. Korn and Ottensmeyer claim that, although the *conclusions* from the NMR data of Boesch *et al.*[18] contradict their model, which is helical in the carboxy-terminal region, the NMR *data* themselves are quite consistent with their proposed structure. The hydrophobic surface of glucagon (the nonpolar residues in segment 22−27) is exposed to the surrounding aqueous environment, and this may be the reason for the instability of its conformation and its tendency to aggregate in concentrated solutions.[22]

There is widespread agreement that glucagon exhibits biexponential decay kinetics with decay times of about 1 and 3−4 ns [1.1 (1.3) and 3.6 (3.8) ns at pH 7, room temperature;[23] 0.5 and 3.3 ns at pH 8.15;[24] 1.11 and 3.26 ns at pH 8.2, 25 °C;[25] 1.54 and 4.08 ns at pH 7.4, 20 °C;[26] 0.83 and 3.53 ns at pH 7.2, 20.0 °C [27]]. Although the dual emission is thought to reflect the presence of different conformers of the indole ring or the existence of differing peptide chain conformations,[25] no one has been able to establish the role of excited-state processes in the origin of the biexponential decay kinetics, because until recently the necessary data analysis approach[3] to do so was not yet available.

In this paper we investigate the photophysics of the polypeptide hormone glucagon in aqueous phosphate buffer (pH 6.7, 17.2 °C) using the scanning procedure in global compartmental analysis. It will be demonstrated how a distinction can be made between reversible and irreversible processes in the excited state. We will show that the dual exponential fluorescence decays of the single tryptophan residue in glucagon originate from two excited-state species which do not interconvert during the fluorescence time scale.

Fluorescence Decay Kinetics

Consider a dynamic, linear, time-invariant, concentration independent (i.e., intramolecular) system consisting of two distinct types of excited-state species with added quencher as depicted in Scheme 1. Ground-state species 1 may reversibly transform into ground-state species 2. Excitation by light creates the excited-state species 1* and 2* which can decay by fluorescence (F) and nonradiative (NR) processes. The composite rate constants for these processes are denoted by k_{0i} ($=k_{Fi} + k_{NRi}$) for species i*. The rate constant describing the transformation 1* → 2* is represented by k_{21}, whereas the conversion 2* → 1* is characterized by k_{12}. In the case of irreversible systems (i.e., systems with k_{21} and/or k_{12} equal to zero), three kinetic models depicted in Schemes 2A,B and 3 are possible. The added quencher Q accelerates the depopulation of the excited states of species i* by k_{Qi}[Q][i*]. For all

SCHEME 1

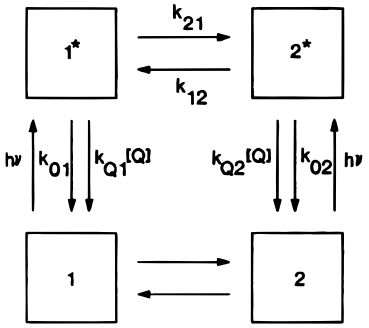

SCHEME 2

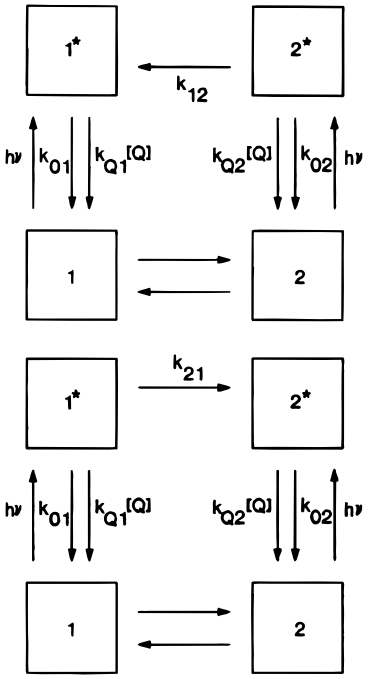

SCHEME 3

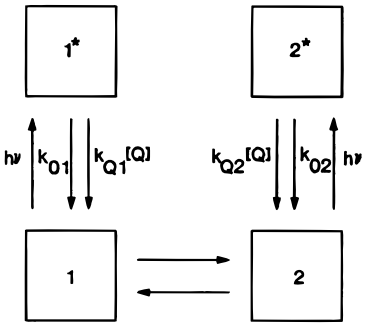

considered cases it is assumed that Q affects exclusively the excited-state species deactivation and does not change in any way the ground-state equilibrium. Furthermore, the quenching is assumed to be of the Stern−Volmer type (i.e., no diffusion-mediated quenching effects are observable).

If the systems depicted in Schemes 1−3 are excited by a δ-pulse which does not significantly alter the concentrations of the ground-state species, the fluorescence δ-response function, $f(\lambda^{em},\lambda^{ex},t)$, measured at emission wavelength λ^{em} with excitation at λ^{ex} is expressed by[28]

$$f(\lambda^{em},\lambda^{ex},t) = \kappa\tilde{\mathbf{c}}(\lambda^{em})\mathbf{U}\exp(t\Gamma)\,\mathbf{U}^{-1}\tilde{\mathbf{b}}(\lambda^{ex}) \quad t \geq 0 \quad (1)$$

with κ a proportionality constant. $\mathbf{U} = [\mathbf{U}_1, \mathbf{U}_2]$ is the matrix of the two eigenvectors of matrix $\mathbf{A}$, and $\mathbf{U}^{-1}$ is the inverse of $\mathbf{U}$. γ_1 and γ_2 are the eigenvalues of $\mathbf{A}$ corresponding to $\mathbf{U}_1$ and $\mathbf{U}_2$, and $\exp(t\Gamma) = \mathrm{diag}\{\exp(\gamma_1 t), \exp(\gamma_2 t)\}$. The matrices $\mathbf{A}$ according to Schemes 1−3 are given by eqs 2−4, respectively:

$$\mathbf{A} \equiv \begin{bmatrix} -(k_{01} + k_{21} + k_{Q1}[Q]) & k_{12} \\ k_{21} & -(k_{02} + k_{12} + k_{Q2}[Q]) \end{bmatrix} \quad (2)$$

$$\mathbf{A} \equiv \begin{bmatrix} -(k_{01} + k_{21} + k_{Q1}[Q]) & 0 \\ k_{21} & -(k_{02} + k_{Q2}[Q]) \end{bmatrix} \quad (3a)$$

$$\mathbf{A} \equiv \begin{bmatrix} -(k_{01} + k_{Q1}[Q]) & k_{12} \\ 0 & -(k_{02} + k_{12} + k_{Q2}[Q]) \end{bmatrix} \quad (3b)$$

$$\mathbf{A} \equiv \begin{bmatrix} -(k_{01} + k_{Q1}[Q]) & 0 \\ 0 & -(k_{02} + k_{Q2}[Q]) \end{bmatrix} \quad (4)$$

$\tilde{\mathbf{b}}(\lambda^{ex})$ is the 2×1 vector with elements $\tilde{b}_i(\lambda^{ex})$ defined by[29]

$$\tilde{b}_i = b_i/(b_1 + b_2) \quad (5)$$

where b_i denotes the concentration of i^* at time zero,

$$b_i = [i^*]_{t=0} \quad (6)$$

which, in the low excitation limit and when the absorbance of species i is low (<0.1) and Beer's law is valid, is proportional to the ground-state absorbance of i. The elements $\tilde{b}_i$ depend on λ^{ex} and can be linked in a global analysis over decay traces collected at the same excitation wavelength.

The 1×2 vector of the normalized emission weighting factors $\tilde{c}_i$ of species i^* at λ^{em} is denoted by $\tilde{\mathbf{c}}$, which depends on λ^{em} and can be linked over decay curves obtained at the same emission wavelength,[28]

$$\tilde{c}_i = c_i/(c_1 + c_2) \quad (7)$$

Equation 1 can be written in the common biexponential format:

$$f(\lambda^{em},\lambda^{ex},t) = \alpha_1 \exp(\gamma_1 t) + \alpha_2 \exp(\gamma_2 t) \quad t \geq 0 \quad (8)$$

The preexponential factors α_i are dependent on k_{01}, k_{21}, k_{02}, k_{12}, k_{Q1}, k_{Q2}, [Q], $\tilde{b}_1$, and $\tilde{c}_1$. The exponential factors γ_i are related to the decay times τ_i according to

$$\gamma_i = -1/\tau_i \quad (9)$$

and are functions of k_{Q1}, k_{Q2}, and [Q] and S_1, S_2, and P defined as[3]

$$S_1 = k_{01} + k_{21} \quad (10a)$$

$$S_2 = k_{02} + k_{12} \quad (10b)$$

$$P = k_{21}k_{12} \quad (10c)$$

For the kinetic models according to Schemes 2 and 3, eq 10 can be simplified.

Species-Associated Emission Spectra (SAEMS)

The contribution of species i^* to the total steady-state fluorescence spectrum $F(\lambda^{em},\lambda^{ex})$ at emission wavelength λ^{em} with excitation at λ^{ex} is called the species-*a*ssociated *em*ission spectrum, $\mathrm{SAEMS}_i(\lambda^{em},\lambda^{ex})$, and is given by[28]

$$\mathrm{SAEMS}_i(\lambda^{em},\lambda^{ex}) = \Omega_i(\lambda^{em},\lambda^{ex})F(\lambda^{em},\lambda^{ex}) \quad (11a)$$

with

$$\Omega_i = [\tilde{c}_i(\lambda^{em})(\mathbf{A}^{-1}\tilde{\mathbf{b}}(\lambda^{ex}))_i]/[\tilde{\mathbf{c}}(\lambda^{em})\mathbf{A}^{-1}\tilde{\mathbf{b}}(\lambda^{ex})] \quad (11b)$$

with $\mathbf{A}^{-1}$ the inverse of matrix $\mathbf{A}$.

If and only if $k_{21} = k_{12} = 0$ (Scheme 3), one has that[29]

$$\mathrm{DAS}_i(\lambda^{em},\lambda^{ex}) = [\alpha_i(\lambda^{em},\lambda^{ex})\tau_i/\sum_j \alpha_j(\lambda^{em},\lambda^{ex})\tau_j]F(\lambda^{em},\lambda^{ex}) = \mathrm{SAEMS}_i(\lambda^{em},\lambda^{ex}) \quad (12)$$

where $\mathrm{DAS}_i(\lambda^{em},\lambda^{ex})$ is the decay-associated emission spectrum of species i^*.[30]

In that case the ratio of the SAEMS or DAS yields

$$\frac{\mathrm{SAEMS}_1(\lambda^{em},\lambda^{ex})}{\mathrm{SAEMS}_2(\lambda^{em},\lambda^{ex})} = \frac{\mathrm{DAS}_1(\lambda^{em},\lambda^{ex})}{\mathrm{DAS}_2(\lambda^{em},\lambda^{ex})} = \frac{\Omega_1}{\Omega_2} = \frac{\tilde{b}_1\tilde{c}_1\tau_1}{\tilde{b}_2\tilde{c}_2\tau_2} = \frac{\tilde{b}_1\phi_{F1}}{(1-\tilde{b}_1)\phi_{F2}}\frac{\int_{\Delta\lambda^{em}}\rho_1(\lambda^{em})\,d\lambda^{em}}{\int_{\Delta\lambda^{em}}\rho_2(\lambda^{em})\,d\lambda^{em}} \quad (13)$$

τ_i (eq 14) and ϕ_i (eq 15) are the lifetime and fluorescence quantum yield, respectively, of species i^*:

$$\tau_i = 1/(k_{0i} + k_{Qi}[Q]) \quad (14)$$

$$\phi_{Fi} = k_{Fi}/(k_{0i} + k_{Qi}[Q]) = k_{Fi}\tau_i \quad (15)$$

k_{Fi} is the rate constant of fluorescence for species i^*. $\Delta\lambda^{em}$ is the emission wavelength interval around λ^{em} where the fluorescence signal is monitored. $\rho_i(\lambda^{em})$ is the emission density of i^* at emission wavelength λ^{em} normalized to the complete SAEMS_i of i^*. $\rho_i(\lambda^{em})$ is defined by[28]

$$\rho_i(\lambda^{em}) = \mathrm{SAEMS}_i(\lambda^{em},\lambda^{ex})/\int_{\text{full emission band}}\mathrm{SAEMS}_i(\lambda^{em},\lambda^{ex})\,d\lambda^{em} \quad (16)$$

Experimental Methods

Chemicals. Glucagon [Sigma, from mixture of bovine and porcine pancreas, +95% (HPLC)] was used as received. Na_2HPO_4 (Acros Organics, ACS reagent) and NaH_2PO_4 (Acros Organics, ACS reagent) were used without further purification to prepare the buffer solutions in Milli-Q water (Millipore Co.). Glucagon concentrations were well below 10^4 M (typically < 2×10^{-5} M), at which glucagon is in the monomeric form.[31] NaI (Acros Organics, 99.99%) was used as such in the quenching experiments. NaCl (Aldrich, +99.99%) was used to keep the ionic strength of the solutions constant whereas

$Na_2S_2O_3$ (Aldrich, +99.99%, anhydrous) was used to prevent oxidation of iodide by air oxygen. *p*-Terphenyl (Merck, scintillation grade) in methanol (Fluka, spectroscopic grade) quenched with NaI was the reference compound in the single-photon timing experiments.[32−34]

Instrumentation and Data Analysis. The pH of the buffer solutions was determined with a Radiometer Copenhagen PHM82 standard pH meter. Fully corrected fluorescence spectra were recorded with a Spex Fluorolog 212. Fluorescence decay traces were collected at 17.2 °C by the single-photon timing method,[35,36] using the 295 nm excitation of a synchronously pumped, cavity-dumped, frequency-doubled Rhodamine 6G dye laser. The reference convolution method used iodide-quenched *p*-terphenyl in methanol as a reference.[32−34] In the analyses the reference lifetime was kept fixed at its known value (0.11 ns).

The global compartmental analysis of the fluorescence decay surface of species undergoing excited-state processes was implemented in the existing general global analysis program[12] based on Marquardt's[37] algorithm. For intramolecular two-state excited-state processes with added quencher, the global fitting parameters are k_{01}, k_{21}, k_{02}, k_{12}, k_{Q1}, k_{Q2}, $\tilde{b}_1(\lambda^{ex})$, and $\tilde{c}_1(\lambda^{em})$. In addition each decay curve has one local fitting parameter. A description of the program implementation of global compartmental analysis has been given elsewhere.[38] The fitting parameter values were estimated by minimizing the global reduced χ_g^2, subject to constraints on the values of the fitting parameters:

$$\chi_g^2 = \sum_l^q \sum_i w_{li}(y_{li}^o - y_{li}^c)/\nu \qquad (17)$$

Here the index l sums over q experiments and the index i sums over the appropriate channel limits for each individual experiment. y_{li}^o and y_{li}^c denote respectively the *o*bserved (experimental) and *c*alculated (fitted) values corresponding to the *i*th channel of the *l*th experiment, and w_{li} is the corresponding statistical weight. ν represents the number of degrees of freedom for the entire multidimensional fluorescence decay surface. It is crucial that all fitting parameters be subject to simple range constraints on their values. The problem of minimizing χ_g^2 can be stated mathematically as follows:

$$\text{minimize } \chi_g^2(x) \text{ for all } x \quad x \in R^n$$

$$\text{subject to } s_j \le x_j \le t_j \quad j = 1, 2, ..., n \qquad (18)$$

with n the number of adjustable parameters. This format assumes that upper and lower constraints exist on all fitting parameters. Restrictions on the values of a particular fitting parameter j can be removed by allowing very large negative and positive values for respectively s_j and t_j. For all rate constants s_j was set at -0.01 ns^{-1}; for the local scaling factors (see Scheme 4) s_j was set at 0. The default constraints on $\tilde{b}_1$ and $\tilde{c}_1$ are $-0.5 < (\tilde{b}_1, \tilde{c}_1) \le 1.5$. Small negative s_j prevent oscillations in the nonlinear least-squares search which would occur if the values of the fitting parameters were forced to be non-negative.

The numerical statistical tests incorporated the calculation of χ_g^2 and its corresponding $Z\chi_g^2$:

$$Z\chi_g^2 = (0.5\nu)^{1/2}(\chi_g^2 - 1) \qquad (19)$$

Using $Z\chi_g^2$ the goodness-of-fit of analyses with different ν can be readily compared. The additional numerical and graphical statistical criteria to judge the quality of the fits were described elsewhere.[36]

SCHEME 4

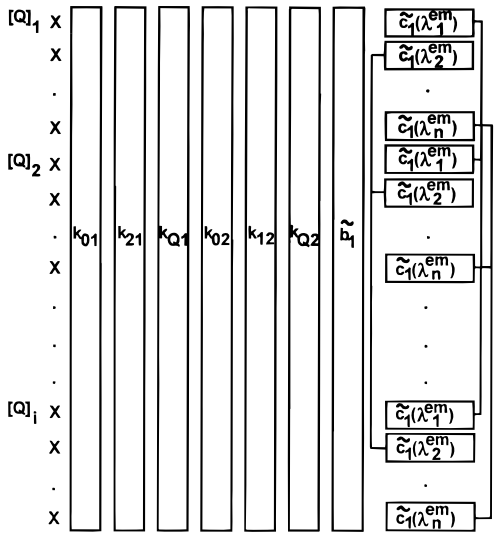

TABLE 1: Decay Times and Corresponding Standard Deviations of Glucagon in Aqueous Phosphate Buffer (pH 6.7, 17.2 °C) Estimated by Global Biexponential Analysis with Decay Times Linked over all λ^{em} at Each [I$^-$]

[I$^-$] (M)	τ_i (ns)	τ_2 (ns)	χ_g^2	$Z\chi_g^2$	no.[a]
0	0.99 ± 0.01	3.71 ± 0.01	1.080	5.485	20
0.1	0.71 ± 0.01	2.83 ± 0.03	1.006	0.168	5
0.2	0.54 ± 0.01	1.75 ± 0.01	1.063	2.035	7

[a] Number of curves analyzed together.

To determine the intervals of the rate constants k_{ij}, series of global compartmental analyses were performed in which (at least) one of the rate constants k_{ij} was kept constant at different preset values while the remaining fitting parameters were allowed to vary freely (i.e., the scanning procedure).[3] The decay parameters were linked as shown in Scheme 4. Boxed parameters are linked while X denotes the local scaling factors.

The quoted errors are one standard deviation.

Results

The time-resolved fluorescence of glucagon was recorded at three different sodium iodide concentrations ([Q] = 0, 0.1, and 0.2 M) in aqueous phosphate buffer (pH 6.7 and 17.2 °C) as a function of emission wavelength. The samples were excited at λ^{ex} = 295 nm, ensuring that only the Trp residue in glucagon is excited. The emission wavelength λ^{em} at [I$^-$] = 0 M was varied from 340 to 440 nm in 5 nm intervals, whereas at [I$^-$] = 0.1 and 0.2 M the emission was collected in the 350−410 nm region in steps of 10 nm. For [Q] = 0 M the time increment was 30 ps/channel, while for [Q] = 0.1 and 0.2 M 15 ps/channel was used as timing calibration. All decays were collected in $^1/_2$K channels of a multichannel analyzer. The ionic strength of solutions with different [I$^-$] was kept constant by addition of NaCl.

The decay curves collected at the same iodide concentration but at differing λ^{em} were analyzed together as biexponentials with linked decay times according to eqs 8 and 9. The decay times $\tau_{1,2}$ estimated at different [I$^-$] are compiled in Table 1. All decays had positive preexponential factors.

In the next step 29 decay traces collected at different λ^{em} and iodide concentrations were analyzed together with global

compartmental analysis using the scanning procedure. The linking of the parameters is given in Scheme 4. Rate constant k_{01} was scanned (i.e., kept fixed at various preset values) from 0.01 to 1.20 ns^{-1}, whereas the other fitting parameters were freely adjustable. The plot of $Z\chi_g^2$ as a function of k_{01} (figure not shown) indicates that the $Z\chi_g^2$ values remain practically constant up to $k_{01} = 1.10$ ns^{-1} after which $Z\chi_g^2$ increases. Plateaus were found for the rate constants k_{02} ($\approx$0.267 ns^{-1}) and k_{12} ($\approx$0 ns^{-1}) as a function of k_{01} for k_{01} values smaller than 1.00 ns^{-1}, whereas k_{21} decreases linearly with increasing k_{01} (figure not shown). The parameters S_1, S_2, and P also remain constant for values of k_{01} up to 1.00 ns^{-1}. The value of P averaged over the plateau is practically zero [$\langle P\rangle = (6 \pm 3) \times 10^{-5}$ ns^{-2}], indicative of an irreversible excited-state process. Visual inspection of the plots of S_1, S_2, and P as a function of k_{01} yields a value of 1.00 ns^{-1} as upper limit on k_{01}. The limits on the rate constants k_{ij} are calculated according to eq 20, where

$$0 < k_{01} < \langle S_1 - P/S_2\rangle \tag{20a}$$

$$\langle P/S_2\rangle < k_{21} < \langle S_1\rangle \tag{20b}$$

$$0 < k_{02} < \langle S_2 - P/S_1\rangle \tag{20c}$$

$$\langle P/S_1\rangle < k_{12} < \langle S_2\rangle \tag{20d}$$

$\langle\ \rangle$ denotes the average of the respective expressions calculated with the plateau values of S_1, S_2, and P. The errors on the limits are computed as the sample standard deviations. This results in the following boundaries on k_{ij}: $k_{01} < 1.020 \pm 0.007$ ns^{-1}, $(2 \pm 1) \times 10^{-4} < k_{21} < 1.020 \pm 0.007$ ns^{-1}, $k_{02} < 0.2666 \pm 0.0006$ ns^{-1}, $(6 \pm 3) \times 10^{-5} < k_{12} < 0.2667 \pm 0.0006$ ns^{-1}. The upper limit on k_{01} computed according to eq 20a is in excellent agreement with the visually determined one. The values of $\tilde{b}_1$ as a function of k_{01} are different from zero or one and therefore conclusively show that at $\lambda^{ex} = 295$ nm two ground-state species of glucagon are excited. Plateaus are also found for the quenching rate constants as a function of k_{01}. The average plateau values of k_{Q1} and k_{Q2} are 2.36 $\pm$ 0.03 and 1.71 $\pm$ 0.05 M^{-1} ns^{-1}, respectively, indicating that the decay component of 1 ns is quenched to somewhat larger extent than the 3.7 ns component.

For the same fluorescence decay surface k_{02} was scanned from 0.001 to 0.29 ns^{-1} with the other fitting parameters freely adjustable. Plateaus were found for $Z\chi_g^2$; the rate constants k_{01}, k_{21}, k_{Q1}, and k_{Q2}, and S_1, S_2, and P as a function of k_{02} for k_{02} values up to 0.27 ns^{-1}. This upper limit on k_{02} is in agreement with that determined by scanning k_{01}. Again P was found to be very small [$\langle P\rangle = (1 \pm 1) \times 10^{-5}$ ns^{-2}]. The following rate constant limits were obtained using eq 20: $k_{01} < 1.0139 \pm 0.0006$ ns^{-1}, $(3 \pm 4) \times 10^{-5} < k_{21} < 1.0139 \pm 0.0006$ ns^{-1}, $k_{02} < 0.269\,81 \pm 0.000\,05$ ns^{-1}, $(0.6 \pm 1) \times 10^{-5} < k_{12} < 0.269\,82 \pm 0.000\,05$ ns^{-1}. These limits are the same as when k_{01} was scanned. The values of k_{Q1} and k_{Q2} averaged over the plateau are 2.64 $\pm$ 0.07 and 1.26 $\pm$ 0.02 M^{-1} ns^{-1}, respectively.

Scanning the rate constants k_{01} or k_{02} resulted in the same average plateau values of S_1, S_2, and P and the same limits on the rate constants k_{ij}. The analyses also indicate that P is zero within experimental error. In this case two kinetic models are possible: (i) $k_{21} = 0$ *or* $k_{12} = 0$ (Scheme 2A,B); (ii) $k_{21} = 0$ *and* $k_{12} = 0$ (Scheme 3). To distinguish between these two different kinetic models, k_{01} (respectively k_{02}) was scanned while k_{12} (respectively k_{21}) was held fixed at zero. The other fitting parameters were allowed to vary freely.

In a first series of repetitive global compartmental analyses k_{01} was scanned from 0.01 to 1.20 ns^{-1} with $k_{12} = 0$. Plateaus were found in the plots of $Z\chi_g^2$, k_{02} (= S_2), k_{Q1}, k_{Q2}, and S_1 as a function of k_{01} up to $k_{01} = 1.00$ ns^{-1}. Figure 1 shows k_{02} (= S_2), k_{21}, and S_1 as a function of k_{01}. The values of k_{21} decrease linearly with increasing k_{01} in this range. The visually determined upper limit on k_{01} is in agreement with that found in previous scannings. The value of k_{02} is uniquely determined ($k_{02} = \langle S_2\rangle = 0.269 \pm 0.001$ ns^{-1}) whereas the average plateau values of S_1 ($\langle S_1\rangle = 1.009 \pm 0.001$ ns^{-1}) specifies the upper limit on k_{01} and k_{21}. The upper limits on k_{01} and k_{21} are in perfect agreement with previously determined ones. The values of k_{Q1} and k_{Q2} averaged over the plateau are 2.5 $\pm$ 0.2 and 1.23 $\pm$ 0.03 M^{-1} ns^{-1}, respectively.

The same fluorescence decay traces were subsequently analyzed with k_{02} scanned while k_{21} was held fixed at zero (figures not shown). The rate constant k_{12} decreases linearly with increasing k_{02} up to a value of 0.27 ns^{-1}, whereas the parameters k_{01} (=S_1) and S_2 have constant values in the same range of k_{02}. The average plateau value of S_1 ($\langle S_1\rangle = 1.008 \pm 0.001$ ns^{-1}) specifies the value of k_{01}, whereas $\langle S_2\rangle = 0.271 \pm 0.005$ ns^{-1} sets the upper limit on the rate constants k_{02} and k_{12}. The values of $\tilde{b}_1$ vary as a function of k_{02} in the range of constant S_1, S_2, and P. The average values of k_{Q1} and k_{Q2} as a function of k_{02} are 2.70 $\pm$ 0.05 and 1.27 $\pm$ 0.01 M^{-1} ns^{-1}, respectively.

Since both series of analyses with scanned k_{01} (with $k_{12} = 0$) and k_{02} (with $k_{21} = 0$) give excellent fits as judged by $Z\chi_g^2$, the DAS (eq 12) should be compared with the SAEMS (eq 11) to establish the correct kinetic model for glucagon in aqueous phosphate buffer.[3]

The SAEMS in the absence of iodide calculated from the global compartmental analysis with $k_{01} = 1$ ns^{-1} and $k_{12} = 0$ ns^{-1} are shown in Figure 2. The SAEMS have a similar emission maximum near 345 nm but quite different amplitudes, in agreement with the DAS reported by Cockle and Szabo.[25] The SAEMS at $k_{21} = 0$ with $k_{12} = 0$, $k_{01} = 0.01$ ns^{-1} with $k_{12} = 0$, at $k_{02} = 0.01$ ns^{-1} with $k_{21} = 0$, and at $k_{02} = 0.26$ ns^{-1} with $k_{21} = 0$ are identical with the previous ones and are therefore not displayed. Hence, the SAEMS are independent of the k_{ij} values within the plateau region. The DAS associated with the globally estimated decay times $\tau_1 = 0.99$ ns and $\tau_2 = 3.71$ ns are identical with the SAEMS. Therefore, one can conclude that the rate constants k_{21} and k_{12} are both equal to zero (Scheme 3 is valid), implying that for monomeric glucagon at pH 6.7 and 17.2 °C the two excited-state species with different lifetimes do not interconvert on the fluorescence time scale. The two excited species are formed by excitation of their respective ground states ($\tilde{b}_1$ different from zero and unity).

Since k_{12} and k_{21} are both equal to zero (Scheme 3 and eq 4 are valid), the photophysical system is uniquely (or globally) identifiable. As a consequence, a single global compartmental analysis in which k_{21} and k_{12} are both held fixed at zero suffices to determine all remaining fitting parameters. Such analysis of 29 decay traces gave an excellent fit ($\chi_g^2 = 1.078$, $Z\chi_g^2 = 5.934$) with the following values for the rate constants: $k_{01} = 1.01 \pm 0.01$ ns^{-1}; $k_{Q1} = 2.73 \pm 0.06$ M^{-1} ns^{-1}; $k_{02} = 0.27 \pm 0.01$ ns^{-1}; $k_{Q2} = 1.28 \pm 0.01$ M^{-1} ns^{-1}. It is evident that k_{01} and k_{02} are the reciprocal values of the lifetimes in the absence of quencher (Table 1). The value of $\tilde{b}_1$ at $\lambda^{ex} = 295$ nm equals 0.84 $\pm$ 0.01. In the low-excitation limit (as in single-photon timing measurements) and when the absorbance is low (<0.1) and Beer's law is valid, one has that

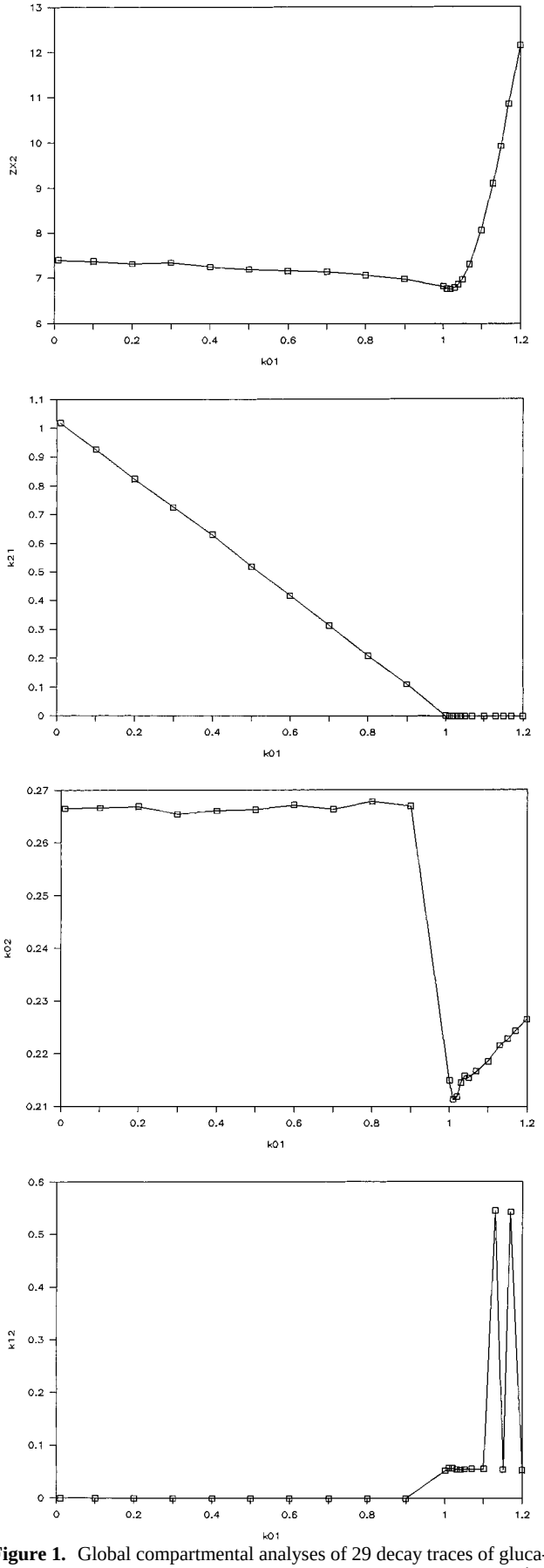

Figure 1. Global compartmental analyses of 29 decay traces of glucagon in aqueous phosphate buffer (pH 6.7 and 17.2 °C) at different λ^{em} and [I^-] as a function of k_{01} with $k_{12} = 0$ with globally estimated values of the rate constants (in ns^{-1}) k_{21} and k_{02} (= S_2). S_1 (in ns^{-1}) calculated from the scanned rate constant k_{01} and the estimated rate constant k_{21}.

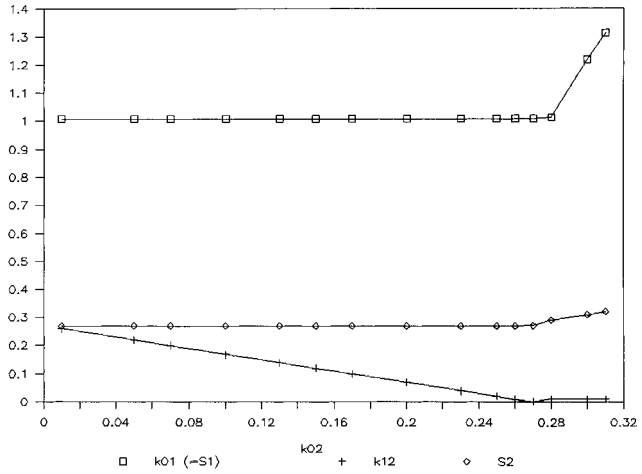

Figure 2. Resolution of the stationary fluorescence spectrum $F(\lambda^{em}, \lambda^{ex} = 295$ nm) of glucagon at pH 6.7 and 17.2 °C in the absence of iodide into the SAEMS associated with species 1* (□, 1 ns) and 2* (■, 3.7 ns) calculated from the global compartmental analysis with $k_{01} = 1\ ns^{-1}$ and $k_{12} = 0\ ns^{-1}$. The propagated errors are within the contours of the plotted symbols.

$$\tilde{b}_1(\lambda^{ex}) = \frac{\epsilon_1(\lambda^{ex})[1]}{\epsilon_1(\lambda^{ex})[1] + \epsilon_2(\lambda^{ex})[2]} \tag{21}$$

yielding $\epsilon_1[1]/\epsilon_2[2] = 5.25 \pm 0.06$. The values of the spectral parameters $\tilde{c}_1$ vary with emission wavelength. The exact values of the rate constants k_{0i} are the upper limits that were obtained in the previous four scannings (scanning k_{01}, k_{02}, and k_{01} with $k_{12} = 0$ and k_{02} with $k_{21} = 0$). From $\tilde{c}_1(\lambda^{em})$ one can obtain the ratio of the fluorescence rate constants, k_{F1}/k_{F2}, provided the SAEMS are available:

$$\frac{\tilde{c}_1(\lambda^{em})}{\tilde{c}_2(\lambda^{em})} = \frac{\tilde{c}_1(\lambda^{em})}{1 - \tilde{c}_1(\lambda^{em})} = \left(\frac{k_{F1}}{k_{F2}}\right)\frac{\int_{\Delta\lambda^{em}}\rho_1(\lambda^{em})\,d\lambda^{em}}{\int_{\Delta\lambda^{em}}\rho_2(\lambda^{em})\,d\lambda^{em}} \tag{22}$$

When the wavelength intervals $\Delta\lambda^{em}$ around λ^{em} are continuous (i.e., they neither overlap nor show interruptions) over the whole emission spectrum, integration of eq 22 over the full fluorescence spectra yields

$$\frac{\sum_{\forall\lambda^{em}}\tilde{c}_1(\lambda^{em})}{\sum_{\forall\lambda^{em}}\tilde{c}_2(\lambda^{em})} = \frac{k_{F1}}{k_{F2}} \tag{23}$$

In that case the ratio k_{F1}/k_{F2} can be obtained from the ratio of the sums of $\tilde{c}_1$ and $\tilde{c}_2$ estimated over the complete fluorescence emission band.

If $k_{21} = k_{12} = 0$ (Scheme 3), the ratio of the fluorescence quantum yields (eq 15) can be obtained by multiplying the ratio k_{F1}/k_{F2} by the ratio of the lifetimes τ_1/τ_2:

$$\frac{\phi_{F1}}{\phi_{F2}} = \frac{k_{F1}}{(k_{01} + k_{Q1}[Q])}\frac{(k_{02} + k_{Q2}[Q])}{k_{F2}} = \frac{k_{F1}}{k_{F2}}\frac{\tau_1}{\tau_2} \tag{24}$$

If $k_{21} = k_{12} = 0$, the total quantum yield of fluorescence ϕ can be expressed as

$$\phi = \tilde{b}_1\phi_{F1} + \tilde{b}_2\phi_{F2} = \tilde{b}_1\phi_{F1} + (1 - \tilde{b}_1)\phi_{F2} \tag{25}$$

The combination of eqs 24 and 25 allows one to calculate values

for ϕ_{F1} and ϕ_{F2}. Combining ϕ_{F1} and ϕ_{F2} with τ_1 and τ_2 (eq 14) yields values for the individual rate constants of fluorescence (k_{Fi}) and nonradiative decay (k_{NR}) for both excited-state species; in other words, one can separate the composite rate constants k_{01} and k_{02} into their constituting components.

The application of eqs 22 and 23 requires integration over the whole emission spectrum. Since $\tilde{c}_1$ values are not available under 340 nm, values at 320, 325, 330, and 335 nm were obtained by extrapolation. The average value of the ratio k_{F1}/k_{F2} calculated according to eqs 22 and 23 equals 0.30. When this value is multiplied by k_{02}/k_{01}, one obtains a value of 0.08 for the ratio ϕ^0_{F1}/ϕ^0_{F2} of the fluorescence quantum yields without (indicated by the superscript 0) added quencher. Using a value of 0.13_3 in eq 25 for ϕ^0 of glucagon in the absence of added quencher,[24] and combining eq 25 with eq 24 results in the following values: $\phi^0_{F1} = 0.047$ and $\phi^0_{F2} = 0.58$. Multiplication of ϕ^0_{Fi} by k_{0i} gives (eq 15) $k_{F1} = 0.05$ ns^{-1} and $k_{F2} = 0.16$ ns^{-1}. Subtracting these values from k_{0i} yields values for the nonradiative rate constants: $k_{NR1} = 0.96$ ns^{-1} and $k_{NR2} = 0.11$ ns^{-1}.

Discussion

All single-curve and global analyses (standard biexponential and compartmental) of the fluorescence decay traces of monomeric glucagon in dilute aqueous solution confirm the biexponential decay kinetics reported previously.[23−27] The lifetime values in the absence of the quencher NaI are in excellent agreement with those reported by Grinvald and Steinberg,[23] Cockle and Szabo,[25] and Chen *et al.*[27] The various analyses of decay traces recorded in the presence of added quencher ([Q] = 0.1 and 0.2 M) show that no diffusion-mediated transient effects are observable. Indeed, a simple Stern−Volmer relationship (eq 14) was found to be adequate for describing each of the fluorescence lifetimes of glucagon as a function of [Q]. The relatively low quencher concentrations and solvent viscosity can rationalize these observations. It cannot be ruled out, however, that, at higher quencher concentrations and/or higher solvent viscosity, diffusion-mediated transients effects will be found and a more complicated model for quenching will have to be employed. The excellent agreement between the results obtained by the different analyses (global biexponential at each [Q] according to eqs 8 and 9 and the various global compartmental analyses) should be emphasized. The positive preexponentials $\alpha_{1,2}$ (eq 8) recovered in the biexponential analyses are compatible with the model depicted in Scheme 3 (matrix **A** given by eq 4), although they cannot be used as proof that this model is the correct one. Indeed, positive preexponential factors may be found for any of the models depicted in Schemes 1−3. Negative preexponentials, on the other hand, are a fingerprint for an excited-state process as depicted in Schemes 1 and 2 and can never be found for the model described by Scheme 3.[3] Since positive preexponentials were always recovered, a compartmental analysis as outlined in the Results section was necessary to pinpoint the correct model for the fluorescence decay kinetics of monomeric glucagon.

The global compartmental analyses in which the rate constants k_{01} and k_{02} are scanned result in extremely small P values, indicative of an irreversible excited-state process. Furthermore, the $\tilde{b}_1$ value different from zero or unity conclusively shows that at $\lambda^{ex} = 295$ nm both ground-state species are excited. Both decay components are efficiently quenched, the decay component of 1 ns being more easily quenched than its 3.7 ns counterpart. The values of the quenching rate constants indicate that the Trp residue in differing conformations or in different peptide chain environments is exposed to the solvent. This is in accordance with the model proposed by Korn and Ottensmeyer which postulates that the nonpolar residues in segment 22−27 are exposed to the surrounding aqueous environment.[22] To distinguish between the two possible models for an irreversible excited-state process [(i) $k_{21} = 0$ *or* $k_{12} = 0$ (Scheme 2A,B) and (ii) $k_{21} = 0$ *and* $k_{12} = 0$ (Scheme 3)], repetitive global compartmental analyses were performed in which k_{01} (respectively k_{02}) was scanned while k_{12} (respectively k_{21}) was held fixed at zero. The comparison of the SAEMS with the DAS allows one to conclude that the model with $k_{21} = 0$ *and* $k_{12} = 0$ (Scheme 3) is the adequate one to describe the time-resolved fluorescence of Trp_{25} in monomeric glucagon. This implies that the two excited-state species with lifetimes of 1 and 3.7 ns do not interconvert on the fluorescence time scale. Hence, the biexponential decays of the single fluorophore Trp_{25} in glucagon do not arise from an excited-state reaction but are consistent with the existence of a ground-state equilibrium.

Heterogeneity in the Trp microenvironment in glucagon could originate from the existence of different local conformers of the tryptophyl residue or from the presence of the two major peptide backbone environments involving Trp_{25} (identified in CD,[16] optically detected magnetic resonance,[19] and ^{1}H NMR studies[17,18,21]) which do not interconvert on the time scale of fluorescence. Although a definitive assignment of the two emission components of the Trp fluorescence of glucagon is somewhat premature, our analysis points to a tentative plausible explanation of the origin of the dual exponential emission of glucagon. The values of the quenching rate constants show that the decay component of 1 ns (species 1*) is more accessible to added quencher than its 3.7 ns counterpart (species 2*). The relatively high values of k_{Qi} are indicative of a Trp residue exposed to the surrounding aqueous environment. The lower value for k_{Q2} is consistent with Trp_{25} in a more shielded environment as provided by the α-helical structure of the carboxy-terminal segment[16,17,19,21,22] or the local nonrandom-chain-fold involving fragment 22−25.[18] The values of ϕ_{F1}, ϕ_{F2}, k_{F1}, and k_{F2} give further support to the assignment of species $1^{(*)}$ to a Trp residue in a flexible extended random coil conformation of the polypeptide chain while species $2^{(*)}$ would correspond to a Trp residue in a compact, quite rigid backbone conformation. Nevertheless, the alternative hypothesis that the two fluorescent components represent local conformers of the Trp sidechain cannot completely be ruled out. To get additional arguments in support of either hypothesis, time-resolved fluorescence anisotropy measurements might be helpful. Tran *et al.* found that the fluorescence anisotropy of glucagon decays biexponentially and at 26 °C the rotational correlation times $\varphi_{1,2}$ are 1.67 ns and 0.31 ns at pH 10.2 and 2.15 ns and 0.52 ns at pH 2.2.[39] These authors attributed the short decay to the restricted motion of Trp while rotation of the whole protein is responsible for the longer decay.

Global analysis of unmatched polarized fluorescence decay traces in which one can test if each lifetime τ_i corresponds to a particular set of rotation lifetimes φ_j should help to establish the origin of the biexponentiality of the fluorescence (anisotropy) of monomeric glucagon.[40] The value of the ratio $\epsilon_1[1]/\epsilon_2[2] = 5.25$ calculated from $\tilde{b}_1$ shows that ground-state species 1 absorbs more light at 295 nm than species 2. Note that the ratio $[1]/[2] \approx 4$ estimated by Boesch *et al.*[18] is in line with the fact that species 1 absorbs more light than species 2, provided ϵ_2 is not too much different from ϵ_1.

Conclusions

The use of the scanning procedure in global compartmental analysis allows one to distinguish reversible from irreversible transformation processes in the excited state.[3] We have shown that by comparing the species-associated with the decay-associated emission spectra a distinction can be made between a unidirectional process in the excited state (Scheme 2) and the case where no interconversion occurs between the two excited-state species (Scheme 3). Since Scheme 3 is shown to be valid, the described global compartmental analysis estimates in a single step values for all model parameters, i.e., k_{01}, k_{02}, k_{Q1}, k_{Q2}, $\tilde{b}_1$, and $\tilde{c}_1$. A more conventional approach, e.g. as in ref 41, does not allow one to distinguish Scheme 2 from Scheme 3, and can only provide information on the model parameters of Scheme 3 after additional calculations. The global compartmental analysis yields this information in a single step, takes into account all correlations between the model parameters, and links the model parameters over the total set of decay traces. Our results confirm the dual exponential character of the time-resolved fluorescence of the single tryptophan residue in polypeptide hormone glucagon at pH 6.7 and 17.2 °C. For glucagon in neutral aqueous phosphate buffer it is shown for the first time, with the use of the global compartmental analysis approach with added quencher, that their biexponential fluorescence decays originate from excitation of two ground-state species to their respective excited states which do not interconvert on the time scale of fluorescence, i.e., $k_{21} = 0$ and $k_{12} = 0$. The composite rate constants, k_{01} and k_{02}, of deactivation of the two excited-state species are resolved into contributions via fluorescence and nonradiative decay. The emission spectra associated with each excited-state species are identical with the decay-associated emission spectra. A single global compartmental analysis with k_{21} and k_{12} held fixed at zero yields values of all remaining fitting parameters.

The data analysis approach described in this paper to elucidate the origin of the biexponential fluorescence decays of glucagon is generally applicable to any intramolecular two-state excited-state process and will be useful for studying peptides and proteins with dual exponential fluorescence decay characteristics.

Acknowledgment. L.V.D. thanks the K.U. Leuven for financial support. N.B. is an Onderzoeksdirecteur of the Fonds voor Wetenschappelijk Onderzoek (FWO).

References and Notes

(1) Beechem, J. M.; Brand, L. *Annu. Rev. Biochem.* **1985**, *54*, 43−71.

(2) (a) Beechem, J. M.; Ameloot, M.; Brand, L. *Chem. Phys. Lett.* **1985**, *120*, 466−472. (b) Ameloot, M.; Beechem, J. M.; Brand, L. *Chem. Phys. Lett.* **1986**, *129*, 211−219.

(3) (a) Van Dommelen, L.; Boens, N.; Ameloot, M.; De Schryver, F. C.; Kowalczyk, A. *J. Phys. Chem.* **1993**, *97*, 11738−11753. (b) Van Dommelen, L.; Boens, N.; De Schryver, F. C.; Ameloot, M. *J. Phys. Chem.* **1995**, *99*, 8959−8971.

(4) Rayner, D. M.; Szabo, A. G. *Can. J. Chem.* **1978**, *56*, 743−745.

(5) Szabo, A. G.; Rayner, D. M. *J. Am. Chem. Soc.* **1980**, *102*, 554−563.

(6) Robbins, R. J.; Fleming, G. R.; Beddard, G. S.; Robinson, G. W.; Thistletwaithe, P. J.; Woolfe, G. J. *J. Am. Chem. Soc.* **1980**, *102*, 6271−6279.

(7) Gudgin, E.; Lopez-Delgado, R.; Ware, W. R. *Can. J. Chem.* **1981**, *59*, 1037−1044.

(8) Chang, M. C.; Petrich, J. W.; McDonald, D. B.; Fleming, G. R. *J. Am. Chem. Soc.* **1983**, *105*, 3819−3824.

(9) Petrich, J. W.; Chang, M. C.; McDonald, D. B.; Fleming, G. R. *J. Am. Chem. Soc.* **1983**, *105*, 3824−3832.

(10) Gudgin, E.; Lopez-Delgado, R.; Ware, W. R. *J. Phys. Chem.* **1983**, *87*, 1559−1565.

(11) Gudgin-Templeton, E. F.; Ware, W. R. *J. Phys. Chem.* **1984**, *88*, 4626−4631.

(12) Boens, N.; Janssens, L. D.; De Schryver, F. C. *Biophys. Chem.* **1989**, *33*, 77−90.

(13) Boens, L. D.; Janssens, L. D.; Van Dommelen, L.; De Schryver, F. C.; Gallay, J. *Time-Resolved Laser Spectroscopy in Biochemistry III*; Lakowicz, J. R., Ed. *Proc. SPIE* **1992**, *1640*, 58−69.

(14) Willis, K. J.; Szabo, A. G.; Kracjarski, D. T. *Chem. Phys. Lett.* **1991**, *182*, 614−616.

(15) Boens, N.; Van Dommelen, L.; De Schryver, F. C.; Ameloot, M. *Time-Resolved Laser Spectroscopy in Biochemistry IV*; Lakowicz, J. R., Ed. *Proc. SPIE* **1994**, *2137*, 400−411.

(16) Panijpan, B.; Gratzer, W. B. *Eur. J. Biochem.* **1974**, *45*, 547−553.

(17) Wagman, M. E.; Dobson, C. M.; Karplus, M. *FEBS Lett.* **1980**, *119*, 265−270.

(18) Boesch, C.; Bundi, A.; Oppliger, M.; Wüthrich, K. *Eur. J. Biochem.* **1978**, *91*, 209−214.

(19) Ross, J. B. A.; Rousslang, K. W.; Deranleau, D. A.; Kwiram, A. L. *Biochemistry* **1977**, *16*, 5398−5402.

(20) McBride-Warren, P. A.; Epand, R. M. *Biochemistry* **1972**, *11*, 3571−3575.

(21) Yi, G. S.; Choi, B. S.; Kim, H. *Biochem. Int.* **1992**, *28*, 519−524.

(22) Korn, A. P.; Ottensmeyer, F. P. *J. Theor. Biol.* **1983**, *105*, 403−425.

(23) Grinvald, A.; Steinberg, I. Z. *Biochim. Biophys. Acta* **1976**, *427*, 663−678.

(24) Werner, T. C.; Forster, L. S. *Photochem. Photobiol.* **1979**, *29*, 905−914.

(25) Cockle, S. A.; Szabo, A. G. *Photochem. Photobiol.* **1981**, *34*, 23−27.

(26) Ross, J. B. A.; Rousslang, K. W.; Brand, L. *Biochemistry* **1981**, *20*, 4361−4369.

(27) Chen, L. X.-Q.; Petrich, J. W.; Fleming, G. R.; Perico, A. *Chem. Phys. Lett.* **1987**, *139*, 55−61.

(28) Ameloot, M.; Boens, N.; Andriessen, R.; Van den Bergh, V.; De Schryver, F. C. *J. Phys. Chem.* **1991**, *95*, 2041−2047.

(29) Boens, N.; Andriessen, R.; Ameloot, M.; Van Dommelen, L.; De Schryver, F. C. *J. Phys. Chem.* **1992**, *96*, 6331−6342.

(30) Wahl, Ph.; Auchet, J. C. *Biochim. Biophys. Acta* **1972**, *285*, 99−117.

(31) Formisano, S.; Johnson, M. L.; Edelhoch, H. *Proc. Natl. Acad. Sci. U.S.A.* **1977**, *74*, 3340−3344.

(32) Libertini, L. J.; Small, E. W. *Anal. Biochem.* **1984**, *138*, 314−318.

(33) Zuker, M.; Szabo, A. G.; Bramall, L.; Krajcarski, D. T.; Selinger, B. *Rev. Sci. Instrum.* **1985**, *56*, 14−22.

(34) Boens, N.; Ameloot, M.; Yamazaki, I.; De Schryver, F. C. *Chem. Phys.* **1988**, *121*, 73−86.

(35) O'Connor, D. V.; Phillips, D. *Time-correlated Single Photon Counting*; Academic Press: London, 1991.

(36) Boens, N. In *Luminescence Techniques in Chemical and Biochemical Analysis*; Baeyens, W. R. G., De Keukeleire, D., Korkidis, K., Eds.; Marcel Dekker: New York, 1991; pp 21−45.

(37) Marquardt, D. W. *J. Soc. Ind. Appl. Math.* **1963**, *11*, 431−441.

(38) Boens, N.; Ameloot, M.; Hermans, B.; De Schryver, F. C.; Andriessen, R. *J. Phys. Chem.* **1993**, *97*, 799−808.

(39) Tran, C. D.; Beddard, G. S.; Osborne, A. D. *Biochim. Biophys. Acta* **1982**, *709*, 256−264.

(40) Crutzen, M.; Ameloot, M.; Boens, N.; Negri, R. M.; De Schryver, F. C. *J. Phys. Chem.* **1993**, *97*, 8133−8145.

(41) Birks, J. B.; Bartocci, G.; Aloisi, G. G.; Dellonte, S.; Barigelletti, F. *Chem. Phys.* **1980**, *51*, 113−120.